Journal of Civil Engineering and Construction Technology Vol. 2(8), pp. 169-188, August 2011
Available online at http://www.academicjournals.org/jcect
ISSN 2141-2634 ©2011 Academic Journals

Full Length Research Paper

Reflectance spectroscopy as a tool to assess the quality of concrete *in situ*

Anna Brook* and Eyal Ben-Dor

Remote Sensing Laboratory, Department of Geography and Human Environment, Tel-Aviv University, Ramat Aviv, P. O. B. 39040, 69978, Israel.

Accepted June 23, 2011

Modern high-performance concrete (HPC) is one of the most versatile, durable, and cost-effective building materials known to man. Its composition has been well-characterized in 'test sample' reports from laboratory specimens and trial castings: however, its internal structure often reveals large differences from that of 'test sample concrete'. Moreover, the test procedure is considered destructive. To resolve specific problems related to global urban environmental indicators, a new approach, including methods for near-real-time analysis and vast coverage, is required. The use of reflectance spectroscopy across the visible near- and short-infrared spectral region (400 to 2500 nm) was suggested as a tool to assess the status of concrete *in situ*. To examine this technique's potential, several controlled experiments were conducted in which concrete was spectrally measured after applying several treatments, including use of different matrix components and post-curing, ageing and corrosion processes. More than 3000 collected samples revealed that spectral measurement combined with spectral analysis tools provides significant and accurate information on the concrete's status. The spectral models were applied to spatial information obtained using a ground image spectrometer. It was concluded that the suggested tool provides near-real-time information on concrete status and might serve as an innovative application in civil engineering.

Key words: High-performance concrete, hydration, curing, hardening, diffuse reflectance spectroscopy, spectral model.

INTRODUCTION

Modern high-performance concrete (HPC), with its low ratio of water to cementitious material (w/c) is characterized by superior tensile properties and enhanced durability in the face of severe environmental conditions. The literature indicates three main processes in concrete production: hydration, curing, and hardening. Increasing attention toward environmental aspects of material conversion has driven research into modifications that might better meet the increasing demand for sustainability in the construction sector. Such modifications involve the use of additives and changing the composition of the cement (Lura et al., 2009). Many different experimental techniques have been employed to investigate the effects on material conversion. Vicat measurements are often employed to determine setting times (Lura et al., 2009). At later stages in the hydration process, an ultrasonic cement analyzer determines changes in the elastic modulus of the mortar (Ljungkrantz et al., 1994; Malhotra et al., 2004). Calorimetry is employed to monitor the heat released upon hydration (Malhotra and Carino, 2004), whereas X-ray diffraction (Stepkowska, 2002), nuclear magnetic resonance (Richardson, 2000) and Fourier transform infrared spectroscopy (FTIR) are used to obtain chemical information.

Morphological information may be obtained by means of scanning electron microscopy and transmission electron microscopy (Richardson, 2000). A microscopy-based method has also been developed to estimate the w/c ratio of unknown mixtures and degree of hydration (Wong and Buenfeld, 2009). Chemical studies of concrete and cement commonly make use of diffuse-

*Corresponding author. E-mail: anna.brook@gmail.com.

Table 1. Spectral data set of concrete samples.

Data set	Properties	Number of objects
Data set 1	Different matrix components (standard and non-standard component ratio)	1800
Data set 2	Different periods of time for the curing process	1250
Data Set 3	Influence of liquid hardeners	650

spectroscopy methods (Lura et al., 2009). It thus appears that HPCs are well characterized for their composition and mechanical properties, usually documented in 'test sample' reports from laboratory specimens and trial castings. However, the internal structure of the HPC often reveals serious differences from that of the 'test sample concrete', because *in-situ* measurements are complicated, if not impossible. In addition, due to the duration of traditional test methods and the need for sample collection, the test procedure is considered destructive.

In diffuse reflectance spectroscopy (DRS), radiation reflected across a selected spectral region is examined with regard to materials' characteristics. The fundamental vibrations of most building materials generate spectral information in the mid-infrared region (2500 to 14,000 nm), and overtones and combination modes in the near and shortwave infrared region (NIR-SWIR, 900 to 2500 nm) (Clark, 1999; Hunt, 1982). Electronic transitions generate spectral information in the visible-near infrared range (VIS-NIR, 400 to 900 nm) (Friedman and Robinson, 2002; Mualem and Friedman, 1991; Wold et al., 2001), which is seen as color and is governed mostly by Fe-bearing minerals. Since the reflectance across 400 to 2500 nm is always below saturation level, it can be used as an inexpensive tool to quantitatively predict the constituents of the material in question (Awiti et al., 2007; Ben-Dor and Banin, 1995; Grace et al., 2002; Islam et al., 2003; Reeves and Van Kessel, 2000; Reeves et al., 2000; Tittonell et al., 2008).

In previous studies, diffuse reflectance-infrared (DR-FTIR) spectroscopy has been used for chemical investigations of concrete, cement and its components. The results of those studies suggested that the DR-FTIR technique is preferred for investigations of that external physico-chemical interference. However, several drawbacks of DR-FTIR make it virtually impossible to perform *in-situ* studies, where water's strong absorption in the mid-IR range and the surface's flatness make it difficult to use the DR techniques. These considerations validate DR-FTIR technique for ex-situ approaches (Ylm'n et al., 2009).

The purpose of the present study was to demonstrate the efficiency of the DRS technique (VIS-NIR-SWIR) for rapid assessment of the status of HPC detected in situ. To examine the potential of the DRS technique, we conducted several controlled experiments in which concrete was spectrally measured, after applying several treatments which included using different matrix components and post-curing, ageing and corrosion processes.

METHODOLOGY

Spectral measurements

The reflectance data set was collected from selected areas of subsamples of each of the concrete surfaces using a ASD "Fieldspec Pro FRQ" (ASD.Inc, Boulder, CO) VNIR-SWIR spectrometer. To keep the spectral measurement constant and stable, the concrete was scanned from below and spectral measurements were acquired by using a high-intensity contact source probe assembly and a white light source (Tungstarn-Halogen), with a Duraplan borosilicate optical-glass and a Spectralon panel as a white reference. The number of spectra for each measurement was 30, which were then averaged to give a sample spectrum. Internally averaged scans were 100 ml/s each. The wavelength-dependent signal-to-noise ratio (S/N) for our instrument was estimated by taking repeat irradiance measurements of a Spectralon white-reference panel over a 10 min interval and analyzing the spectral variation across this period. For each sample, three spectral replicates were acquired and the average was used as the representative spectrum. To represent a continuously large area of the concrete surface, spectral measurements of 3 ′3 cm^2 areas were taken using the contact probe assembly over the entire area. These measurements were gathered into a spectral cube which was later used to generate a spatial view of the concrete indices.

Materials and composition

The prepared data set consisted of 3700 reflectance spectra in the VIS-NIR-SWIR region (365 to 2485 nm) of the concrete surfaces (Table 1).

The general preparation protocol for all of the measured samples of concrete included a standard mixture of the following components: Type-I Portland cement (CEMI 52.5 N), class-F fly ash, lime, solid aggregates (coarse and fine), normal-weight microsilica sand (CEN standard sand) with an average and maximum grain size of 200 µm, and tap water (Figure 1). All of the samples were treated by the same method of internal curing by retaining water on the concrete surface during the early stage of hydration first few hours. After the initial 24 h, the samples, still in their plastic containers, were wrapped in cling film and sealed in plastic bags at 20°C until the age of 250 days.

Three controlled experiments were conducted to yield three different data sets of concrete samples. The specific recipes for the three data sets are summarized in Table 2.

The first experiment (Data set 1) was focused on generating a versatile database characterized by concretes with different matrix components. Thus, we generated two categories of concrete with different mechanical and strength properties as opposed from the mix composition. Two ordinary Portland cement pastes with w/c ratios of 0.25 and 0.50 were prepared using cement complying with CEMI 52.5 N and tap water. After the initial 24 h, the samples, still in their plastic containers, were wrapped in cling film and sealed in

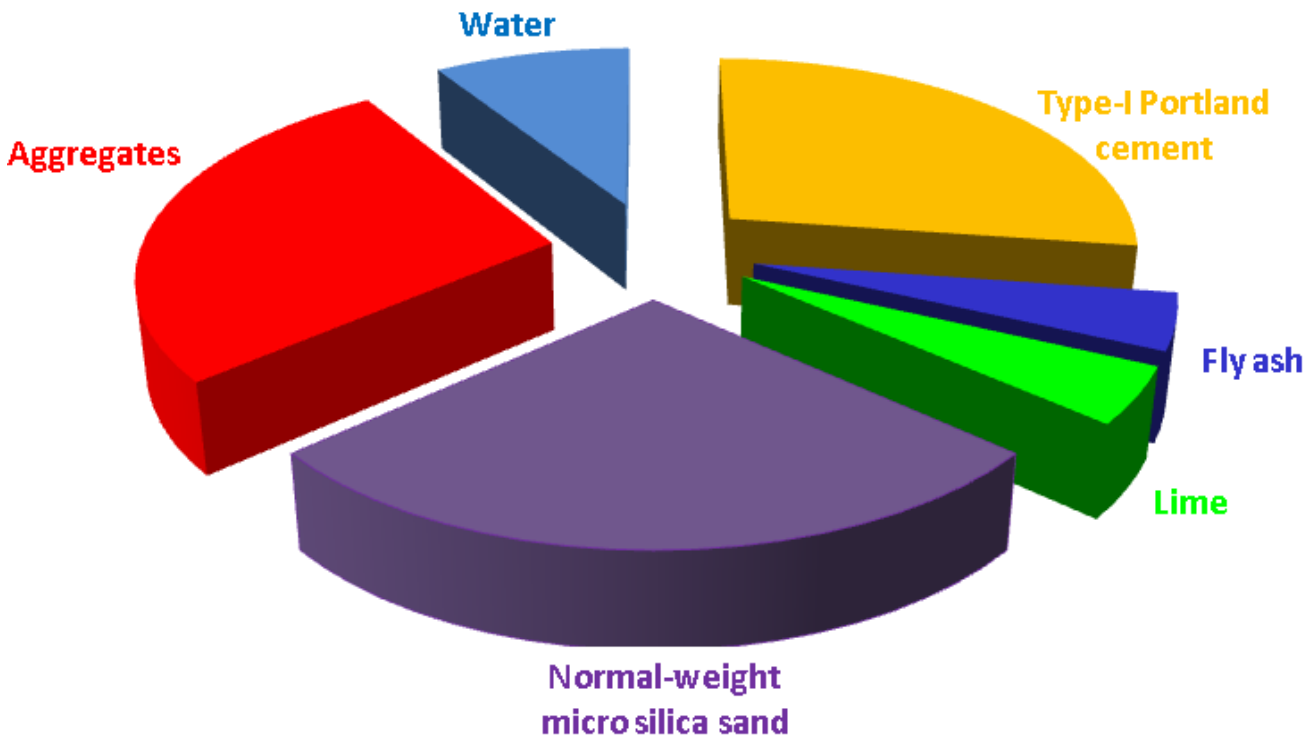

Figure 1. Pie diagram of standard concrete components.

plastic bags at 20°C until the ages of 15, 30, 90, 120 and 250 days.

The second experiment (Data set 2) included four concrete samples that were treated by the same method of internal curing by retaining water on the concrete surface. The difference in each treatment related to the duration of the curing process (0, 3, 5, and 7 days). The samples were spectrally measured of the age of 250 days.

The third experiment (Data set 3) was designed to test the influence of polyvinyl alcohol-acetate (PVAA, Celvol 805 of Celanese Chemicals), an 87 to 89% hydrolyzed polyvinyl acetate, added at different percentages (polymer/cement ratio of 0 to 0.8%), w/c of 0.5 and sand-cement ratio of 3, during the standard 7-day internal curing. All of the polymer solutions formed transparent crack-free films at room temperature. The samples were spectrally measured at the age of 250 days.

Spectral data pre-processing

The spectral calibration process was standardized and normalized using measurements of an internal standard. This process enables the isolation of noisy wavelengths (from the signal) and the generation of a noise-less smooth data set for further analysis. The reflectance spectra of the internal standard and the measured reflectance spectra of the concrete were normalized to the continuum level by interactively choosing continuum points, linearly interpolating between them, and then dividing the final spectrum by the continuum. Equivalent widths (EWs) were measured by choosing the linear boundaries interactively (Figure 2). The average EWs and standard deviation from the mean (σμ) were tabulated (Table 3).

The measure of internal error (σμ) mostly reflects the individual's consistency in choosing the continuum level. From the calculated ratio between continuum-removed spectra (spectral repetitions) of the internal standard, a normalization factor is provided.

Data-classification task

The task of classifying data consists of deciding class membership y' of an unknown data item x' based on a data set (Dreiseitl and Ohno-Mechado, 2002). In this research, as in most problem domains, there is no function relationship y = f(x). Thus, the relationship has to be described more generally by a probability distribution P(x, y); it is then assumed that the data set contains samples independent of P. There are two different approaches to data classification: the first considers only a dichotomous distinction between the two classes, and assigns class labels 0 or 1. The second attempts to model P(y|x) not only as a class label for a data item, but also as a probability of class membership. Logistic regression (LR), artificial neural network (ANN), k-nearest neighbor, and decision tree are algorithmic implementations of ideas from statistical learning theory, which concerns itself with building consistent estimators which perform on a training set (Dreiseitl et al., 2002).

Algorithmically, support vector machines build optimal separation boundaries between data sets by solving a constrained quadratic problem. The disadvantage of support vector machines is that the classification result is purely dichotomous, and no probability of class membership is given (Dreiseitl and Ohno-Machado, 2002; Scholkopf and Smola, 2002).

Classification based on the k-nearest neighbor algorithm differs from the other methods, and here, this algorithm uses the data directly from classification, without building a model first. The major drawback of k-nearest neighbor lies in the calculation of the neighborhood. Thus, a matrix needs to be defined that measures the distance between data items based on trial and error (Dasarathy, 1991; Ripley, 1996).

Decision tree is an algorithm that repeatedly splits the data set according to a criterion that maximizes the separation of the data, resulting in a tree-like structure (Breiman, 2001; Quinlan, 1993). A major disadvantage of the decision tree is in the construction

Table 2. Specific recipes for the three data sets from tested concrete samples.

Data set	Aggregates and sand (in kg)				Water/Cement Ratio	Free air in bulk (%)	Hardener (%)
	Coarse (1-2 cm)	Fine (100-500 mm)	Sand (200 µm)	Fine/coarse ratio			
1	98	48	87	0.5	0.25	1.6	NA
1	98	48	146	0.5	0.5	1.8	NA
2	98	48	87	0.5	0.25	1.5	NA
3	98	48	87	0.5	0.25	1.6	0.1
3	98	48	87	0.5	0.25	2.4	0.2
3	98	48	87	0.5	0.25	4.1	0.3
3	98	48	87	0.5	0.25	4.5	0.4
3	98	48	87	0.5	0.25	5.1	0.6
3	98	48	87	0.5	0.25	5.7	0.8

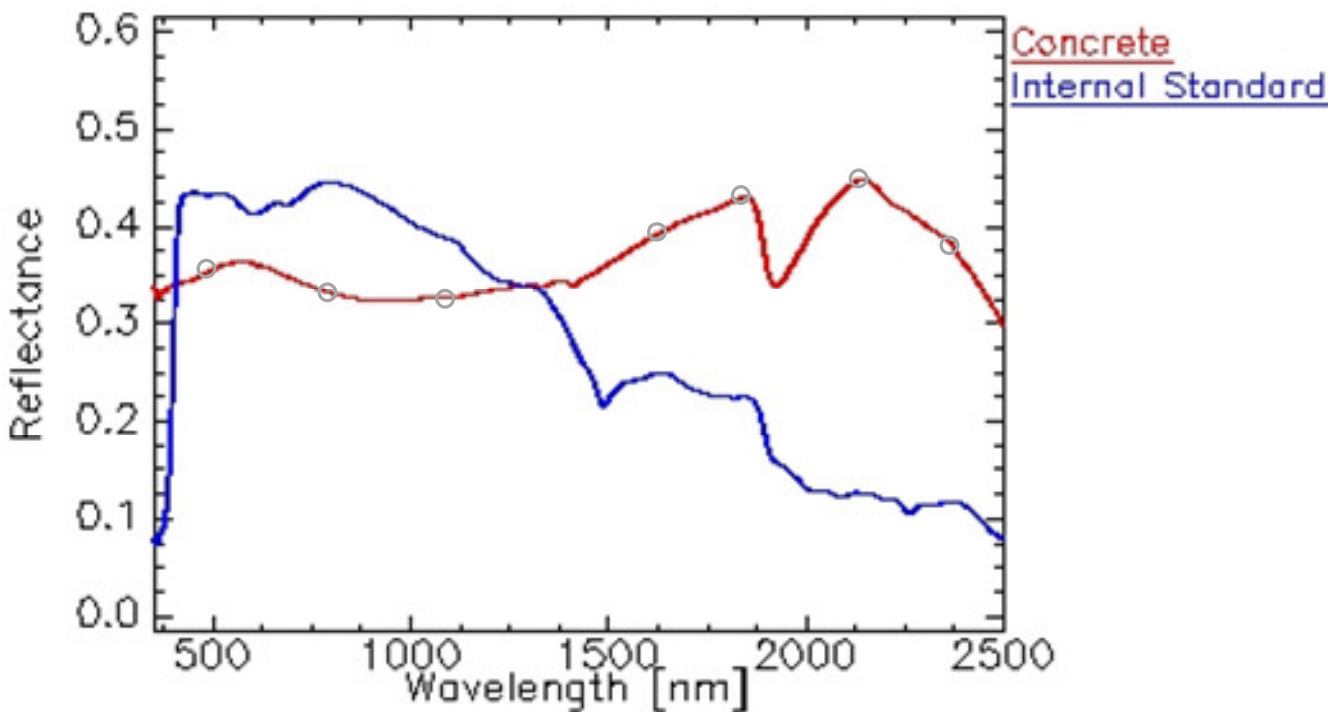

Figure 2. Average reflectance spectrum of concrete (red) and internal standard (blue) with continuum points for the normalization process.

Table 3. Mean absolute error for all reflectance spectra normalized to the continuum level by interactive continuum points.

Parameters	n	λ488 nm	λ 800 nm	λ 1085 nm	λ 1277 nm	λ 1633 nm	λ 1860 nm	λ 2160 nm	λ 2370 nm
Internal standard	879	9.3±0.24	4.9±0.1	1.97±0.06	1.4±0.09	1.32±0.11	0.96±0.01	1.05±0.15	2.3±0.34
Concrete	3700	8.6±0.31	3.9±0.14	0.82±0.1	0.38±0.05	5.45±0.31	6.87±0.24	4.76±0.28	3.95±0.3

process, where at each step, the combination of single best variable and optimal split-point is selected.

LR and ANN models differ from others algorithms in the sense that they both provide a functional (f) form and parameter vector (α) to express $P(y|x) = f(x,\alpha)$. Although the functional forms for the LR and ANN models are quite different, a network without a hidden layer is actually identical to a LR model if the logistic activation function is used.

Input data set for spectral analysis

The spectral models applied at this stage can be trained to weight the significant variables and discount less important ones; nevertheless, we reduced the input data set, since this has proven to enhance overall performance. The data reduction was performed by the following methods: spectral re-sampling, feature-selection algorithms and spectral indices that produce data for the training subset.

The first data set was spectrally re-sampled by box car averaging of three neighboring data points using the Savitzky-Golay algorithm (Savitzky and Golay, 1964) to calculate first and second derivatives of the initial spectra. The simple sample-to-wavelength ratio in the model calibration was a practical data set of 2555 samples versus 717 wavelengths for each spectrum after re-sampling.

Information from the second data set was reduced by parameterization of feature-selection algorithms. The parameterization consists of transforming the signal into a set of feature vectors. The aim of this transformation is to obtain a new representation which is more compact, less redundant, and more suitable for statistical modeling and the calculation of a distance score, or any other kind of score. In a pre-transformation stage, the reflectance spectra were converted to Log(1/R') absorption values (where R' is the reflectance), referred to as multiplicative property. The main transformation techniques, example, principal component analysis (PCA), fast Fourier transformation (FFT), and Haar transform (HT), were selected for the spectral data set after conversion to Log(1/R') values (Figure 3).

PCA transforms the original set of variables by way of an orthogonal transformation to a new set of uncorrelated variables or principal components (PCs) (Clark, 1999). The technique amounts to a straightforward rotation from the original axes to the new ones and of the derivation of PCs in decreasing order of importance. In a successful derivation, a few components account for most of the variation in the original data, but the results of the PCA are strongly dependent on existing variation and uniformity of the data set. The PCA was applied to the Log(1/R')-converted spectral data set (Figure 4) and the scores of all factors with eigenvalues greater than a predefined threshold were used in the spectral model (Geladi and Dabakk, 1995; Osborne et al., 1997).

The FFT, on the other hand, enhances the high frequencies of the spectrum that are generally reduced during the process of obtaining them (Hana et al., 1995). The FFT uses the internal values and, through a second-order interpolation, obtains waveform samples based on a user-specified number of points. The windowing functions can reduce the effects of waveform truncation on the spectral content. FFT was performed by Matlab R2009b (Signal Processing Toolbox).

The HT is a complete set of orthonomal functions, as their partial sum is constantly convergent (Haar, 1910). Thus it is a simple wavelet transformation that provides an adjusted volume of data by normalized average per transformation cycle, performed by Matlab R2009b.

The subspace for sample distribution built by the PCA, FFT and HT was determined only on the training set, and the validation samples were projected in this subspace using pattern files that drive and control the network simulator in batch mode (Table 4).

Finally, spectral indices were calculated based on normalized spectra. The tuning of decision thresholds is very difficult during the processing and verification stages. If the choice of numerical value remains an open issue in the domain, its robustness cannot be verified. This type of uncertainty is a well-known fact in the domain. The choice of normalizing was initially guided by two facts: firstly, in real applications and for text-independent systems, it is easy to compute feature variations; secondly, normalized distribution represents the largest part of the original distribution variance.

The spectra were normalized to an internal standard to minimize measurement instability. The modified reflectance spectra were then manipulated using a continuum removal (CR) technique (Clark and Roush, 1984) (Figure 5). This manipulation enhances high-frequency features while normalizing low-frequency ones. The following features were enhanced: 1. VIS iron oxides (465 nm), 2. IR hygroscopic water (1140 nm), 3. SWIR 1 (1350nm), 4. SWIR 1 hygroscopic water (1450 nm), 5. SWIR 2 liquid water (1940 nm), 6. clay (2220 nm) and 7. calcium (2300 nm).

The input variables from continuum-removed absorption features were reduced through a sequential forward selection (SFS) algorithm (Whitney, 1971). The SFS was the feature-selection technique. This method starts with the inclusion of feature sets one by one to minimize the prediction error of a linear regression model. This stage focuses on conditional exclusion based on feature significance (Pudil et al., 1994). The first step is to use the basic SFS method to select features from the set of available measurements to form of significant feature set. The second step is finding the least significant features in the set. The third step is initialization of the selected algorithm (Step 1) until the feature set obtains its cardinality.

Based on loading scores of the samples from the test set in the PC space, spectral regions were selected to describe the most spectrally active regions within the concrete material. The following features were selected: VIS iron oxides (460 nm), VIS pigment (556 nm), SWIR 1 hygroscopic water (1400 nm), additional hardener (1780 nm), SWIR 2 liquid water (1960 nm), clay (2225 nm), calcium (2309 nm), and hardener (2395 nm). This suggests that despite the monotonous visual spectrum observed for concrete matter, significant spectral information

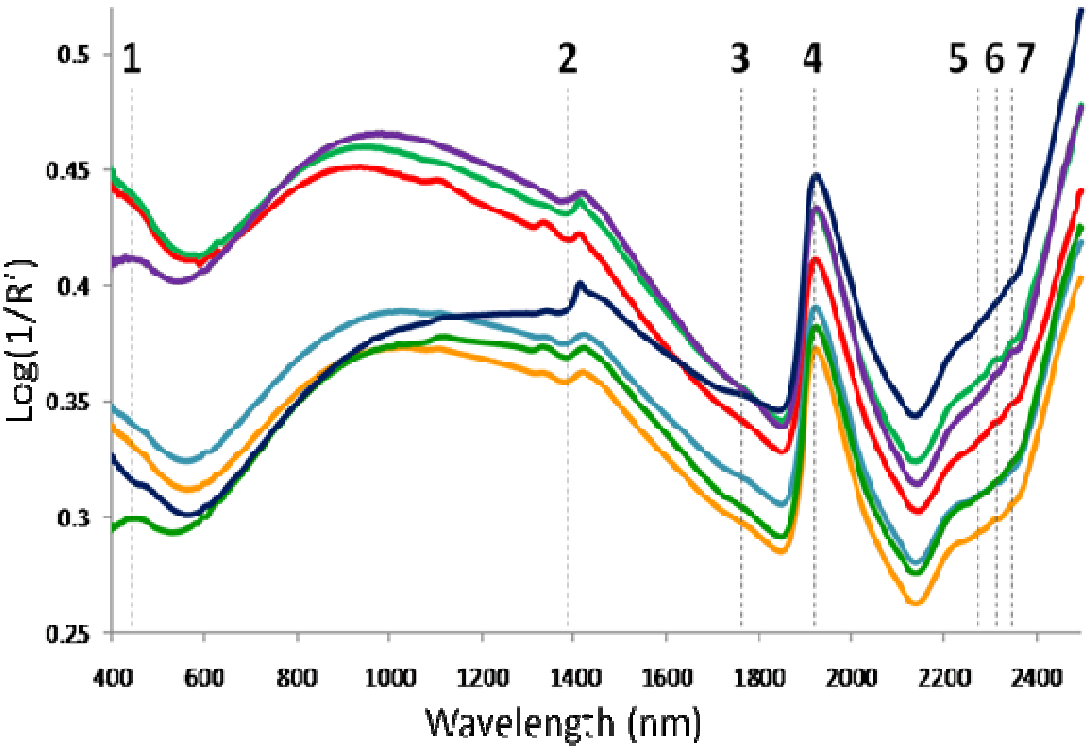

Figure 3. Reflectance spectra converted to Log(1/R') absorption values (R' is the reflectance) where 1 is 460 nm - iron oxide, 2 is 1400 nm - hygroscopic water, 3 is 1780 nm - hardener, 4 is 1930 nm - liquid water, 5 is 2225 nm - clay, 6 is 2309 nm - calcium, 7 is 2395 nm – hardener.

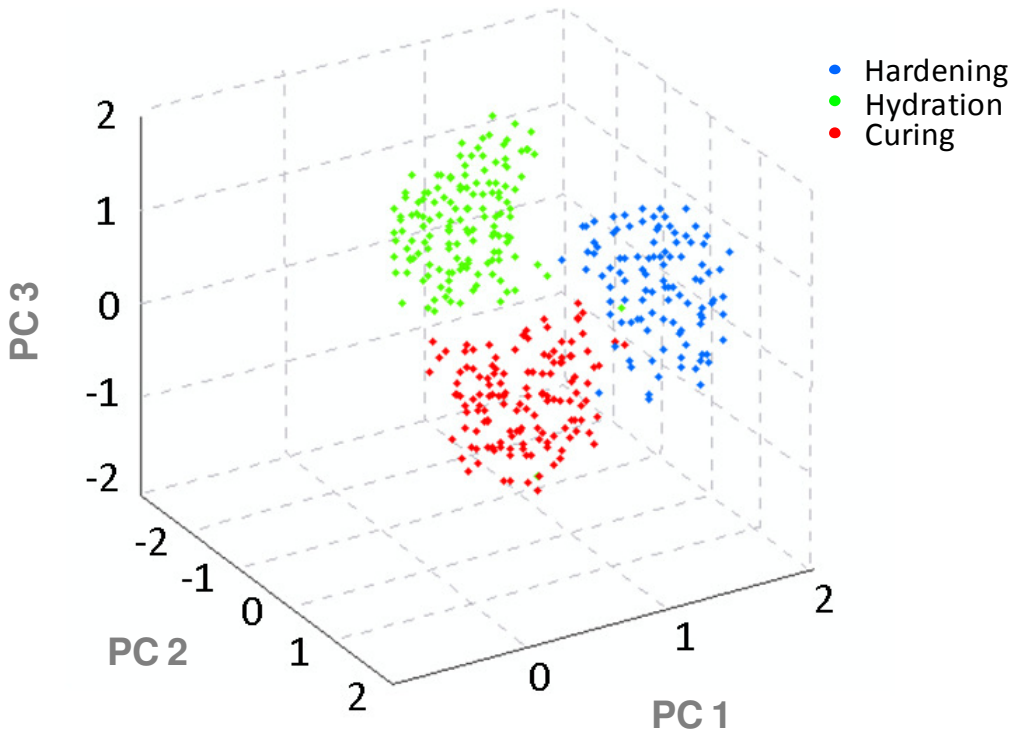

Figure 4. Clustering of concrete samples (hydration, curing and hardening experiments) by the first three principal components (PCs) on Log(1/R')-converted absorption values of reflectance spectra from the training set divided by the D-optimality algorithm.

Table 4. Short description of the features and data sets transformed by selection algorithms.

Feature	Remarks
PCA	PC scores (eight per spectrum)
FFT	FFT coefficients (13 per spectrum)
HT	Third-order HT coefficients (9 per spectrum)

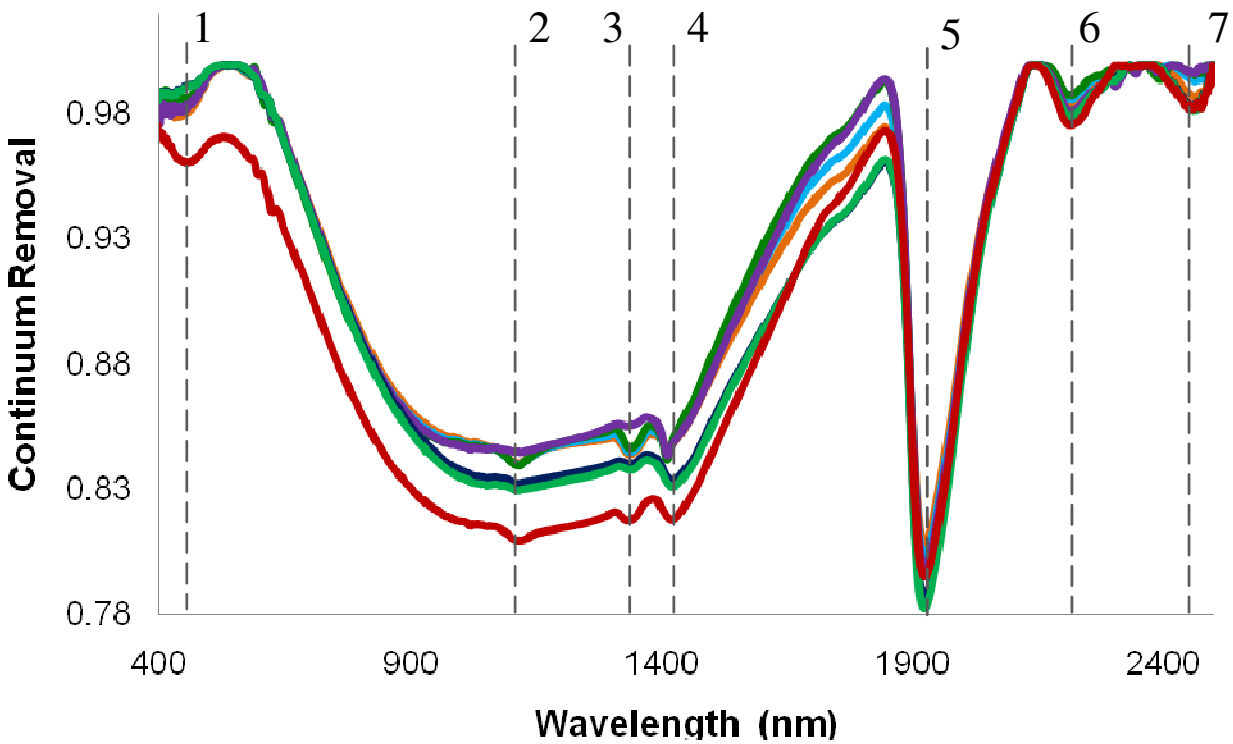

Figure 5. Concrete reflectance spectra manipulated by continuum-removal technique.

does exist within the concrete. It also suggests the need for further spectral analysis to evaluate a spectral model that will predict those parameters.

Aside from the spectral data manipulation, we also applied CR, first derivation (using only absolute values in the calculations), polynomial normalization of spectral curves, and calculation of spectral slopes at certain wavelengths.

The results of the continuum-removed spectra reduced through SFS were: VIS iron oxides (465 nm), NIR hygroscopic water (1140 nm), SWIR 1 (1270nm), SWIR 1 hygroscopic water (1450 nm), additional hardener (1770 nm), SWIR 2 liquid water (1940 nm), clay (2220 nm), calcium (2300 nm), and hardener (2340 nm). An additional spectral index was estimated by Equation (1) in the VIS range. The pigment data in the VIS spectral region were normalized to a range between 0 and 1 using slope calculation of the spectrum:

$$VIS_{slope} = \frac{(610nm - 425nm)}{(610nm + 425nm)} \quad (1)$$

Indirect (inter) correlation of the spectral features across the selected regions and the concrete's properties were examined. Table 5 provides all possible relationships between a property and a spectral response (direct) or a property (indirect). For example, iron oxide was spectrally recognized at 540 and 840 nm and affected the slope of the spectral measurements in the VIS region (400 to 800 nm) (direct). Iron oxides are also correlated to clay content and hence clay content, although having no response in the VIS region, can be correlated to the iron oxide spectral parameters (indirect).

Statistical methods used included multiple analysis of variance (M_ANOVA) to examine group mean differences among the spectral measurements (Huberty and Morris, 1989). Before subjecting them to M_ANOVA, the values of each variable were scaled to a range of 0 to 1. Three M_ANOVA models were used to determine whether the mean values of the spectrally determined variables differed between the processes of concrete hydration, curing and hardening. Bonferroni correction was obtained with confidence intervals. All tests were carried out with up to 120 degrees of freedom.

Table 6 shows the F-statistics of the M_ANOVA model for each process. It presents significant variables, which exceeded the critical value of 5.143, or equivalently, were below the p-value 0.00625, at 0.05 levels under Bonferroni correction. Interpretation for each M_ANOVA model was that means for selected variables differ significantly from one another.

The most practical way to prepare the input data consisted of the

Table 5. Indirect (inter)correlation of spectral regions.

Variable a assignment	Variable B assignment	R square % (correlation coefficient)	Direction
VIS slope	Iron oxides	92.46203	Negative
VIS slope	Liquid water	85.09365	Negative
Iron oxides	Clay	93.94732	Negative
Hygroscopic water	Liquid water	97.50428	Positive
Liquid water	Hardener in SWIR1	96.34285	Negative
Liquid water	Clay	72.5849	Positive
Hygroscopic water	Calcium	78.94835	Positive
Hardener in SWIR 2 region	Calcium	89.57327	Positive
Hygroscopic water	Hardener in SWIR2	73.94361	Positive

Table 6. M_ANOVA results for three models: hydration based on sand-cement ratio, curing, and hardener. The bold numbers are *F*-statistics; italic numbers are p-values.

Variable	Hydration sand/cement ratio		Curing period in days				Hardener percentage	
	High	Low	0	3	5	7	High	Low
N	746	514	220	220	200	200	255	200
VIS slope	27.54, 0.002	7.58, 0.005	34.92,<0.001	21.40, <0.001	28, <0.001	12.75, <0.001	0.59, 0.02	12.75, <0.001
Iron oxides	38.09, <0.001	25.71, <0.001	0.54, 0.273	0.59, 0.073	4.19, 0.13	3.31, 0.009	1.46, 0.09	3.31, 0.009
Hygroscopic water (class)	1.05, 0.105	4.93, 0.384	4.15, 0.145	1.92, 0.341	0.51, 0.341	0.79, 0.341	8.74, <0.001	6.93, <0.001
Hardener in SWIR 1 region	3.46, 0.092	1.97, 0.109	3.91, 0.194	2.57, 0.008	3.15, 0.104	1.87, 0.06	21.49, <0.001	20.51, 0.003
Liquid water	21.73, 0.004	11.41, 0.005	7.73, <0.001	12.37, <0.001	10.73, <0.001	9.36, <0.001	11.06, 0.004	9.92, 0.005
Clay	18.92, <0.001	9.27, 0.006	0.76, 0.352	2.192, 0.384	1.054, 0.139	0.89, 0.07	0.09, 0.24	0.15, 0.2
Calcium	1.97, 0.0724	4.82, 0.0932	5.032, 0.370	1.539, 0.054	1.94, 0.005	1.56, 0.08	5.83, 0.007	5.41, 0.006
Hardener in SWIR 2 region	4.867, 0.052	5.043, 0.194	1.703, 0.130	3.06, 0.093	3.47, 0.23	2.96, 0.154	24.72, <0.001	19.67, <0.001

selection done by the loading scores in the PC space. The results of two other transformation methods (FFT and HT) were based on a larger data set (Table 1). The results of the SFS algorithm were similar to the PCs but failed during the backtracking process, in which the values of the criterion function are always compared to the same feature subset. Thus, tolerance to deviation features in the case of a new object (spectrum) is limited.

Spatial distribution of spectral models

The spatial representation of a continuous large area of concrete surface was achieved by systemically covering 3 x 3 cm^2 areas with spectral measurements using the contact probe assembly to cover the entire area (~40 spectra). These measurements were gathered into a spectral cube that can generate a spatial view of the concrete indices and spectral-based models. The Kriging (Sacks et al., 1989) model is used to interpolate all measured point-source data onto a 3-D surface. The interpolated data cube contains spatial distribution (x/y) of spectral information (z).

The combination of a polynomial model and departures of the form has been suggested as a modeling response (Welch et al., 1990, 1992).

$$y(x) = f(x) + z(x) \quad (2)$$

Where y(x) is the unknown function of interest, f(x) is a known polynomial function of x, and z(x) is the realization of a normally distributed Gaussian random process with zero mean variance σ^2, and non-zero covariance. The f(x) term in Equation (2) is similar to the polynomial model in a response surface and provides a 'global' model of the design space (Sacks et al., 1989).

While f(x) is a 'global' approximation of the design space, z(x) creates 'localized' deviations so that the Kriging model interpolates the n_s sampled data points (spectra). The covariance matrix of z(x) is given by:

Table 7. Analysis of LR estimates for hydration process.

Variable	DF	Parameter estimate	Standard error	Wald chi-square	Pr >chi-square	Standardized estimate	Odds ratio
Intercpt	1	2.4563	0.3942	12.4245	0.0001	-	-
VIS slope	1	-0.9452	0.5984	10.12853	0.0015	0.46397	4.957
Iron oxides	1	-1.0839	0.4738	11.38477	0.0011	0.39483	5.477
Clay	1	1.9908	0.53828	9.372719	0.001	0.47932	4.875

$$\mathrm{Cov}[z(x^i), z(x^j)] = \sigma^2 R[R(x^i, x^j)] \quad (3)$$

Where R is the correlation matrix, and $R(x^i,x^j)$ is the correlation function between any two of the n_s sampled data points x^i and x^j. R is a (n_s | x n_s) symmetric matrix with ones along the diagonal. We employed a Gaussian correlation function of the form:

$$R(x^i, x^j) = \exp \sum_{k=1}^{n_s} \theta_k \left| x_k^i - x_k^j \right|^2 \quad (4)$$

Where θ_k are the unknown correlation parameters used to fit the model, and the x_k^i and x_k^j are the kth components of sample points x^i and x^j. Depending on the choice of correlation function in Equation (2), Kriging can either "honor" the data, providing an exact interpolation of it, or "smooth" the data, providing an inexact interpolation.

LOGISTIC REGRESSION MODEL

In this work, the LR technique (Dreiseitl and Ohno-Mechado, 2002) was used to examine the predictive potential of the reflectance spectra's indication of mechanical properties and processes at the concrete surface. LR was chosen because the independent variables do not have to be normally distributed, or of equal variance within each group.
Three models were constructed using the LR technique:

(1) Hydration predicted by w/c as the original component in the concrete mixture,
(2) Internal curing period predicted by spectral absorption of liquid water in the SWIR2 region,
(3) Hardening predicted by percentage of liquid hardener in the concrete.

Hydration model

The hydration model was based on the w/c ratio in the concrete mixture as provided by the concrete manufacturer (physical property and mixture components). We used 850 spectra for the LR model and 300 spectra to test the hydration model (Data set 1). The sand-to-cement ratio was predicted with three estimated spectral parameters of VIS slope, iron oxides and clay (Table 7). Individual effects in the model were tested by Wald chi²/s, the squared ratio of each parameter divided by its standard error. These tests, shown further on, indicated that all selected spectral features are highly significant.

Hydration model interpretation

The hydration process was evaluated by percentages of w/c and sand-to-concrete ratio within the concrete mixture (Fitted model (1)). This was most easily interpreted by considering the odds ratios corresponding to the parameters: 2 is the increment to log odds for the clay spectral feature in the SWIR 2 region, and the odds ratio 2 = 4.8 indicates that the clay feature is nearly 2.5 times more likely to achieve a better outcome than a hydration model without the clay parameter.

$$P(\text{Hydration})1 = w/c = \frac{1}{1+e^{-(2.4563+1.9908A-1.0839B-0.9452C)}} \quad (5)$$

Where A is clay in SWIR 2, B is iron oxide in VIS, C is the slope in VIS, and D is liquid water in SWIR 2.

The output statement produces a data set containing estimated logit values for each group, and corresponding predicted probabilities of improvement and confidence limits for these probabilities. To plot the predicted probabilities of improvement and confidence limits from the results data set, we selected a spatial interpretation based on a Kriging approach (Figure 6).

The ROC (receiver operating characteristic) curve for the hydration model was calculated from the posterior probabilities of LR analysis (Figure 7). The area under the ROC curve was 0.98, larger than any of the areas obtained when using only a single metrics (Table 8).

Curing period model

The internal curing model was based on actual curing periods of 0, 3, 5 and 7 days at an early concrete age (second experiment, Data set 2). We use 500 spectra for the LR model and 300 spectra to test the curing model. The estimation of liquid water related to the curing process was based on two spectral parameters: VIS slope and liquid water absorption in the SWIR 2 region. Individual effects in the model were tested by Wald chi²/s (Table 9).

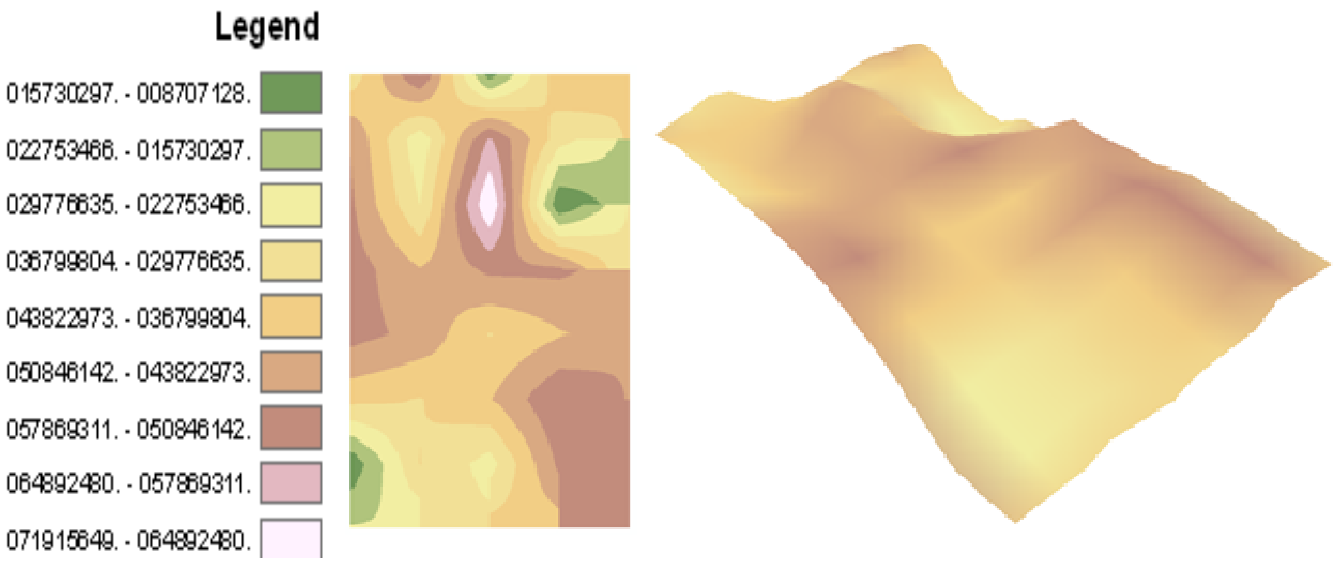

Figure 6. Kriging 3-D map of sand-cement ratio according to Equation (1).

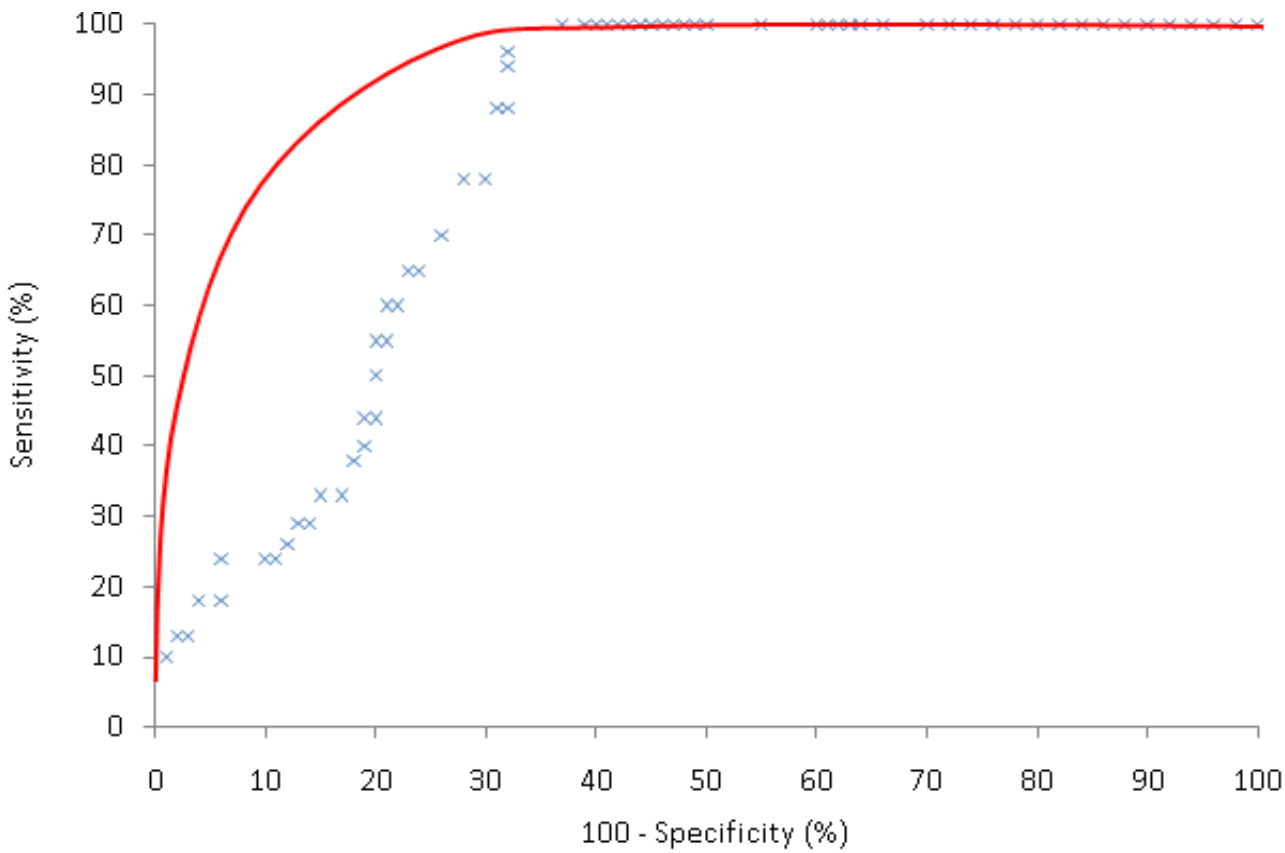

Figure 7. ROC curves calculated for hydration model based on probabilities of LR analysis.

Table 8. Area under ROC curve calculated for LR analysis of each model.

	Hydration	Curing	Hardener
Area under ROC curve	0.98	0.995	0.95

Table 9. Analysis of LR estimates for curing period.

Variable	DF	Parameter estimate	Standard error	Wald chi-square	Pr >chi-square	Standardized estimate	Odds ratio
Intercept	1	15.9435	0.4563	9.47320	0.0115	-	-
VIS slope	1	1.68743	0.1298	11.7637	0.0015	0.3927	2.043
Liquid water	1	2.30556	0.4982	13.0466	0.0001	0.2053	7.309

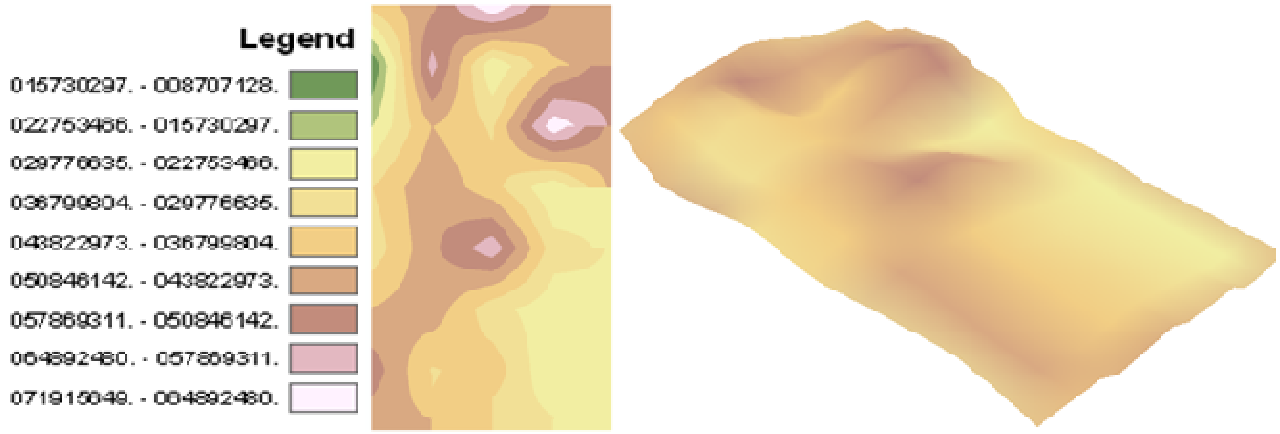

Figure 8. Kriging 3-D map of predicted curing period according to Equation (2).

Curing period model interpretation

The curing period was evaluated by examining the percentage of liquid water in the concrete matrix, which signifies the strength of the concrete (Fitted model (2)). The model was interpreted by the odds ratio of liquid water vs. VIS slope. The odds ratio of liquid water was 2.3 = 7.3, indicating that liquid water absorption is nearly 3.2 times more likely to achieve a better outcome than a curing period model without the liquid water parameter (Figure 8). On the other hand, the odds ratio of the VIS slope was 1.7 = 2, indicating that VIS slope is only 1.17 times more likely to achieve a better outcome. This test indicated that liquid water is a highly significant parameter.

$$P(Curing) = period = \frac{1}{1+e^{-(15.9435+2.30556A+1.68743B)}} \quad (6)$$

Where A is liquid water, B is VIS slope.

Hardener model

The hardener model was based on percentage of liquid hardener added to the concrete matrix in the third

$$P(Hardening) = concentration = \frac{1}{1+e^{-4.2195+7.21569A+3.89022B+0.36021C+12.8642D}} \quad (7)$$

experiment (Data set 3). We used 350 spectra for the LR model and 200 spectra to test the hardener model. The liquid and hygroscopic water estimation was related to the hardening process based on two spectral parameters of hardener features in the SWIR1 and SWIR2 regions. Individual effects in the model were tested by Wald chi²/s (Table 10).

Hardener model interpretation

The hardener percentages were evaluated by examining the percentages of liquid and hygroscopic water in the concrete matrix, which indicate the concrete's strength (Fitted model (3). It is most easily interpreted by considering the odds ratios corresponding to the parameters: 2 is the increment to log odds for the liquid water, and the odds ratio 3.89 = 9.52 indicates that this feature is nearly 2.5 times more likely to achieve a better outcome than a hardener model without the liquid water parameter (Figure 9

Where A is hardener in SWIR 1, B is liquid water in SWIR 2, C is hygroscopic water in SWIR1, D is hardener in SWIR 2.

Table 10. Analysis of LR estimates for hardening process.

Variable	DF	Parameter estimate	Standard error	Wald chi-square	Pr > chi-square	Standardized estimate	Odds ratio
Intercept	1	-4.2195	0.2104	10.0321	0.0015	-	-
Hardener in SWIR1	1	7.21569	0.4932	7.40134	0.0001	0.1932	12.92
Hardener in SWIR2	1	12.8642	0.1023	8.94315	0.001	0.0932	13.92
Hygroscopic water	1	0.36021	0.0022	13.799	0.0015	0.1127	4.32
Liquid water	1	3.89022	0.0143	10.005	0.0105	0.2832	9.52

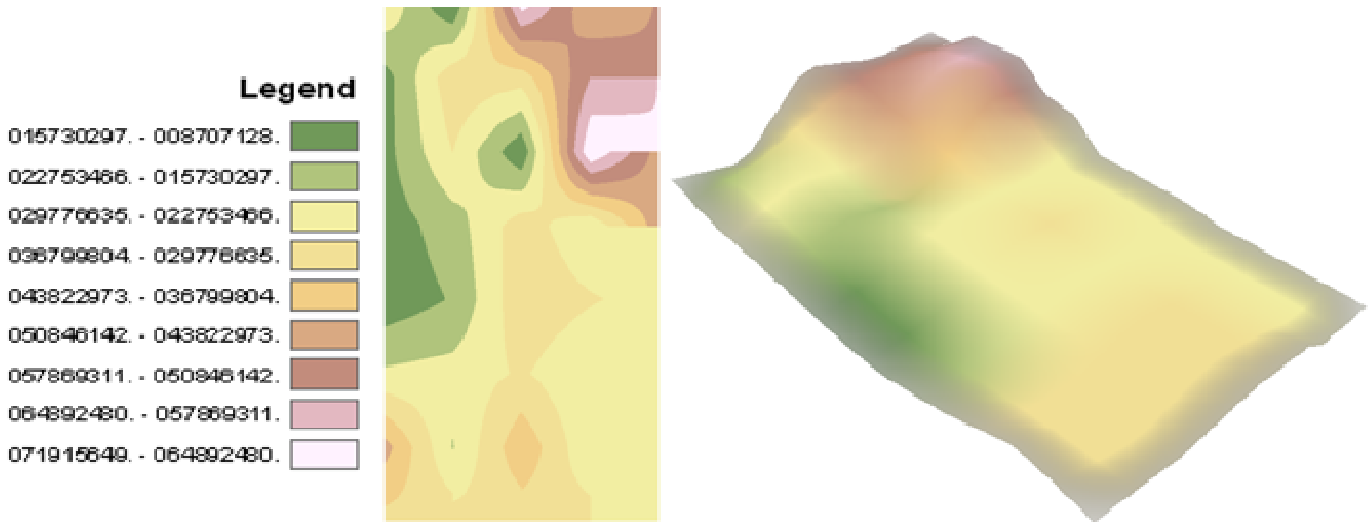

Figure 9. Kriging 3D map of predicted additional hardener according to Equation (3).

ARTIFICIAL NEURAL NETWORK

The ANN applied at this stage can be trained to weight the significant variables and discount the less important ones; nevertheless, we reduced the input data set, since this has been shown to improve overall performance (Zupan and Gasteiger, 1991).

Network topologies

The architecture of an ANN is determined by the way in which the neurons' outputs are connected to other neurons (Despagne and Massart, 1998). We consider layered feed-forward ANNs trained (Sanchez and Sarabia, 1995) with the back-propagation learning algorithm. The network includes three layers of processing stages:

(1). Input distribution,
(2). Layer hidden units (weighted sum of inputs according to nonlinear sigmoid transformation),
(3). Output units (sum of inputs).

Due to nonlinearity in the hidden layers, the output of an ANN is a nonlinear function of the inputs (Udelhoven and Schuttr, 2000). The sigmoid transformation function is subdivided into three separate domains: region with positive second derivative, linear region, and region with negative second derivative. The network was carried out for each class separately. The 2600 concrete spectra (~70% of the objects) chosen from every class constituted the training set (Table 11).

In a classification context, the decision boundary can be nonlinear as well, making the model more flexible compared to multinormal LR (Dreiseitl and Ohno-Mechado, 2002). The optimal number of hidden layers, determined by calculation of the full connection of two layers in which single hidden units were effectively inserted, generally varied between 10 and 20% of the input nodes.

The number of input nodes is reduced according to the range of weights and has to be adaptive as the number of nodes in a hidden layer is fixed. If all weights of one output are large (total range associated), then its variable plays an important role in the network. Thus, the variables can be reduced in terms of network performance (Borggaard and Thodberg, 1992).

The output layer, in which quality of the concrete materials was coded in one output unit, provided

Table 11. Spectral data set (size of the training and test sets) of concrete samples.

Categories	Data set
Number of objects	3700
Training set	2600
Test set	1100
Iterations (epochs)	500-3000
Prediction ability (%)	90-100

information on hydration stage, curing period in the early stage, and spatial distribution of liquid hardening on the surface.

The data of the training set were subjected to PCA, with the first seven PCs taken into consideration. The main goal of net training was to minimize the root Mean square error (RSME Equation 8) and to avoid over fitting.

$$RMSE = \frac{\sum_{i=1}^{N}\sum_{j=1}^{g}(y_{ij} - out_{ij})^2}{Ng} \quad (8)$$

Where y_{ij} is the element of target matrix ($N \times g$) for the data considered training or testing sets, and out_{ij} is the element of the ANN matrix ($N \times g$).

The performance of the network was tested every 200 epochs during the training, and the weights for which the minimal RMSE for the test set was observed and recorded. The back-propagation training algorithm contributes information to the learning algorithm that is able to build a complex relationship between input and output data sets. Thus, the local schemes where the signs of partial derivatives of error measurements are used for determining the directions of weight update. The error modification function helps avoid overfitting of the model during training if it has too many weights (adjustable parameters). To speed up back-propagation, the following techniques were used: batching operation, adaptive learning rate and momentum. In batching operation, multiple input vectors may be applied simultaneously, and a network response is obtained to each of them. Adaptive learning requires that weights receive fortification during back-propagation of the error values through the network (Mutanga and Skidmore, 2004). Thus, the most important weights have high values of derivatives of the error function, while weights which do not change are decreased to zero. If the new error is less than the old error, the learning rate is increasing. Momentum decreases back-propagation sensitivity to small details such as spectral systematic noises in the error and helps to avoid attaching to low minima (Kokaly and Clark, 1999; Mutanga et al., 2003).

The final output of the network can be evaluated in two different ways: 1. the object can be considered as correctly classified if the largest output, regardless of its absolute value, is observed on a node signaling the correct class, or 2. the object can be considered as correctly classified if the largest output is observed on a node signaling the correct class and its value is higher than a predefined threshold. A local out-of-N code was used for output classes encoding labels. In this study, we determined a node dependence minimum threshold of 0.5 (the number of correctly classified objects of the training and test set divided by the total number of objects) that allows soft modeling of data.

Design of the training set

The architecture of the network was optimized for the data divided into training and test sets by he D-optimality algorithm (Choueiki and Mount-Campbell, 1999). In our work, the D-optimal design cannot be directly applied because of the singularity of the information matrix (Cohn, 1996). Therefore, the Log(1/R')-converted spectra were pretreated by PCA (Figure 3). The number of variables was reduced to n'-1 variables. Thus, X becomes a score matrix for n' objects and n'-1 variables. Then we applied the D-optimality method to select objects for the network (Equation 9):

$$y = \sum \beta_i x_i + e \quad (9)$$

Where x_i is the latent variable i

Table 12 summarizes the RMSE results from testing each trained ANN model on an identical data set. It is very clear from the ANN RMSE results that the methodology for selecting the input data and the size of the training data set have an impact on ANN performance. Avoiding over-learning/fitting, a cross-validation data set was launched while training the network (Cohn, 1996). This additional data set, however, was not used in estimating the weights of the ANN model, but rather to identify when to stop training.

The results of the ANOVA of the data in Table 4 were summarized in Table 5. Examining the results in Table 13, we observe that the ANN modeling appears to benefit from selecting a training data set using a D-optimal design. Since the D-optimal factor (Equation 9) is not statistically significant, the ANN model is robust to the spectral complexity within a given restricted region. The size of the training data set has a significant impact on ANN performance. Thus, as expected, when the size of the training data set increases, ANN performance

Table 12. Experimental design and RMSE results.

Source	Training	Components	N	RMSE
PCA	D-Optimal	8	2000	0.0049
PCA	D-Optimal	5	2300	0.0052
PCA	D-Optimal	4	2600	0.0053
FFT	D-Optimal	13	1800	0.094
HT	D-Optimal	9	1000	0.172
Savitzky-Golay	D-Optimal	84	860	0.186
Continuum removal reduced through SFS	D-Optimal	9	1300	0.165

Table 13. ANOVA results.

Source	Degree of freedom	Mean square	F-value
PCA	3	0.0001	0.85
PCA	2	0.0004	1.15
PCA	2	0.0008	1.9
FFT	4	0.0164	165.3
HT	3	0.0386	0.001
Savitzky-Golay	24	0.0256	1025.61
Continuum removal reduced through SFS	3	0.0058	0.15

improves.

Artificial neural network results

We used a fixed structure in which input and output values were scaled between 0.1 and 0.9 by variable. Then the back-propagation learning rule with adaptive learning rate (fixed at 0.1) and momentum (fixed at 0.2) were used.

The scale of weights used in the network can be plotted as a diagram that displays the elements of the weight matrix with areas proportional to their scale. The bias vector is separated from main weights by a vertical line. This diagram displays the element of the weight matrix that stays proportional to their magnitude. The sum of the weights connected to the node can approximate the importance to a well-performing network (Figure 10). Table 14 presents the results of the optimization of the network architecture for the data set: a 95% correct result is obtained for the network with four input nodes (the first four PCs) and three nodes in the hidden layer.

To examine and understand the performance of the network, the correlation structure of the estimated chemical characteristics and processes is important, since ANNs make use of the correlation structure among intercorrelated variables. The performance of the network with eight inputs, and three hidden and three output nodes (8 ′3 ′3) is presented in Figure 11 by calculated RMSE and percentage of correct classification (success rate) of back-propagation with adaptive learning algorithm and momentum. The weights of input nodes 6 to 8 are smaller and suggest that PCs 5 to 7 do not contribute to the network's performance. However, the prediction rates decrease when the number of hidden nodes decreases to two (the first four PCs). Therefore, the best possible structure for the data is four nodes (the first four PCs) and three hidden layers. The optimal network with final weights is presented in Figure 12.

The performance of the optimal network (4 ′3 ′3) presented in Figure 13 does not decrease compared to the first model presented (8 ′3 ′3) in Figure 11. This indicates that the number of input variables can be reduced without changing the performance of the network (effective only in the case of good performance).

The validation stage (Table 15) measure performance of the model by mean square error (MSE), mean prediction error (MPE), and a final total accuracy of the model. In summary, the ANN algorithms appear to achieve consistently high accuracies. The proposed network provides three outputs that evaluate and assess the status of the concrete. These outputs score each of the three dominant processes (hydration, curing and hardening) involved in concrete production. The hydration process, assessed as a quantitative evaluation of the cement-sand ratio, could be interpreted qualitatively as low, medium and high, with high relating to a well-integrated concrete product. The effectiveness of curing is estimated as the period of time that this procedure takes in days. The hardening process as hydration can be assessed by quantitative evaluation of liquid hardeners in the original concrete mixture, or it can be

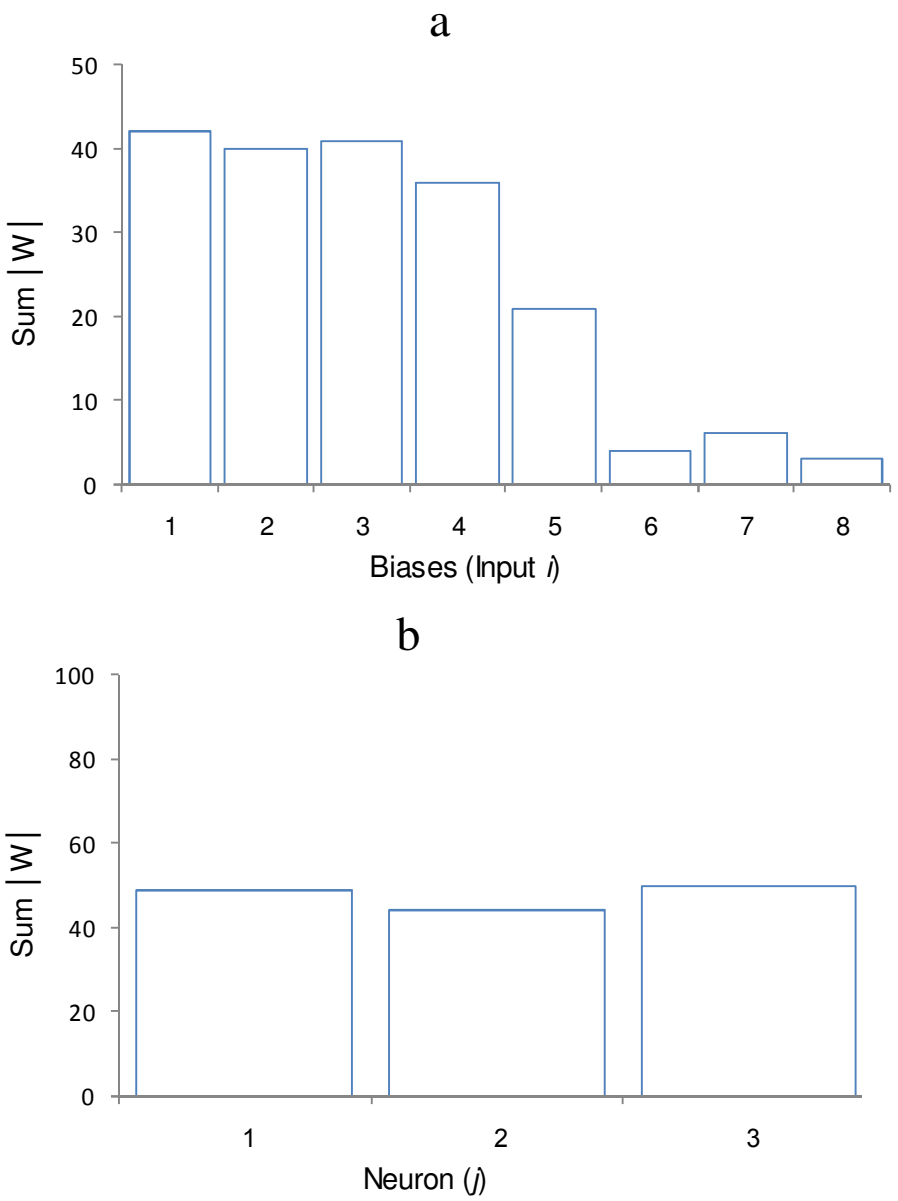

Figure 10. (a) Sum of absolute values of the weights of eight nodes in the input layer (eight input nodes). (b) Sum of the absolute values of the weights of three nodes in the hidden layer.

qualitatively interpreted as low, medium and high with respect to existing standards.

DISCUSSION

The present complex classification problem of concrete's mechanical properties—hydration, curing and hardening—led to parameter-poor models with excellent generalization properties. With LR, model complexity is low, especially when variable transformations (e.g. Log(1/R') and PCA) are used. A modification which enhances the generalization properties of ANNs is the consideration of a weight-decay term.

The LR model collects variables based on schematic selection which is used to remove spurious covariates. If computationally feasible, it should include interaction terms to make the model more flexible. The optimal ANNs is assumed to be the simplest one that achieves the minimum error on the test set. From the available data, we determined that the network with three hidden units is the optimum for all different sets of features. The advantage of using PCs in the context of ANNs, however, is rapidity, since the dimensionality of the input data is

Table 14. Correct results (%) for training and test data sets. Data selected with the D-optimality algorithm; 3000 epochs.

Input nodes	Hidden nodes	Training (correct rate %)	Test (correct rate %)	Output nodes
First 8 PCs	3	100	100	3
First 5 PCs	3	99	95.7	3
First 4 PCs	3	98.6	95.1	3
First 4 PCs	2	82.9	79.5	3

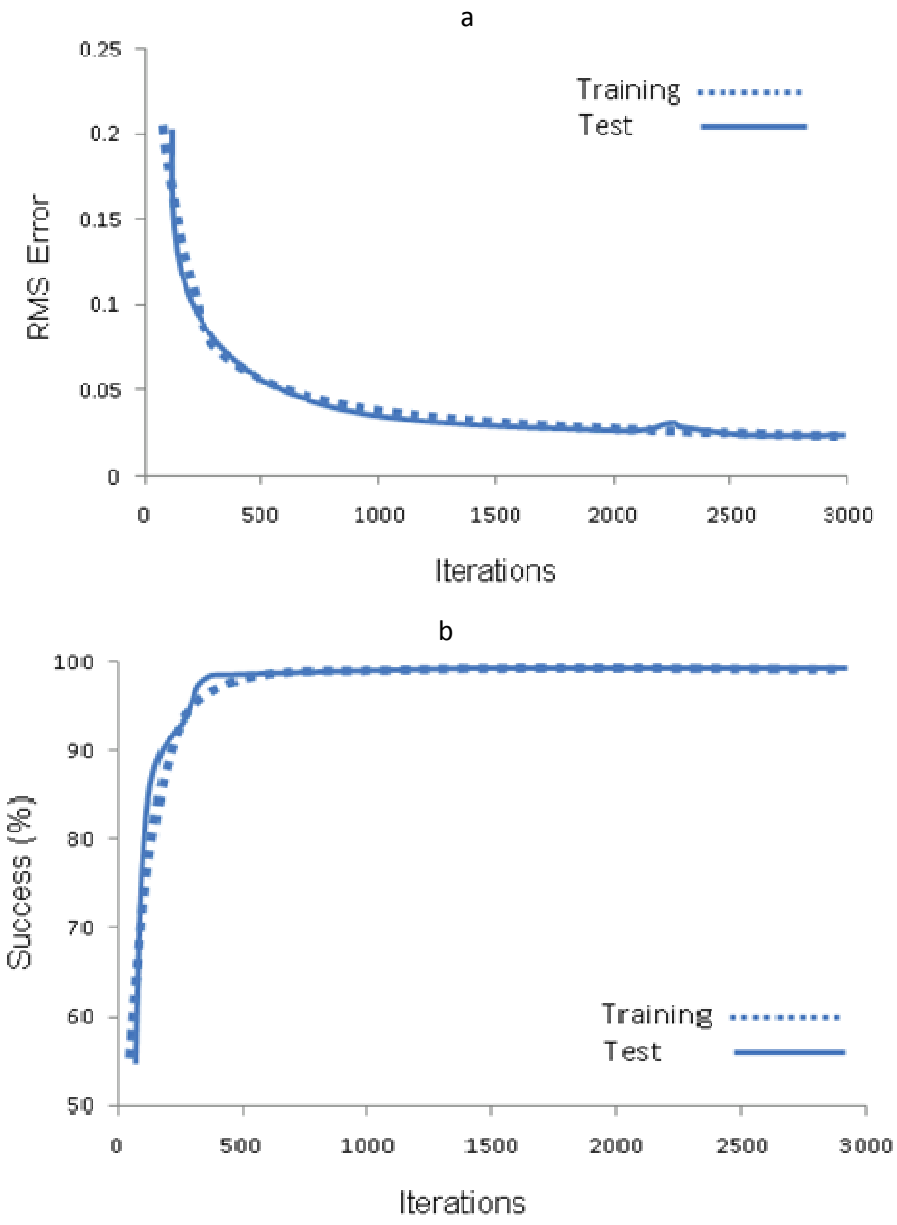

Figure 11. Network of eight input, three hidden and three output nodes. (a) RMSEas a function of the number of training iterations. (b) Correctly classified targets as a function of number of training iterations

reduced (Wise et al., 1995). The ratio between the number of trainable weights and available samples is important, since it strongly influences the generalization property of the ANN (Riedmiller and Braun, 1993).

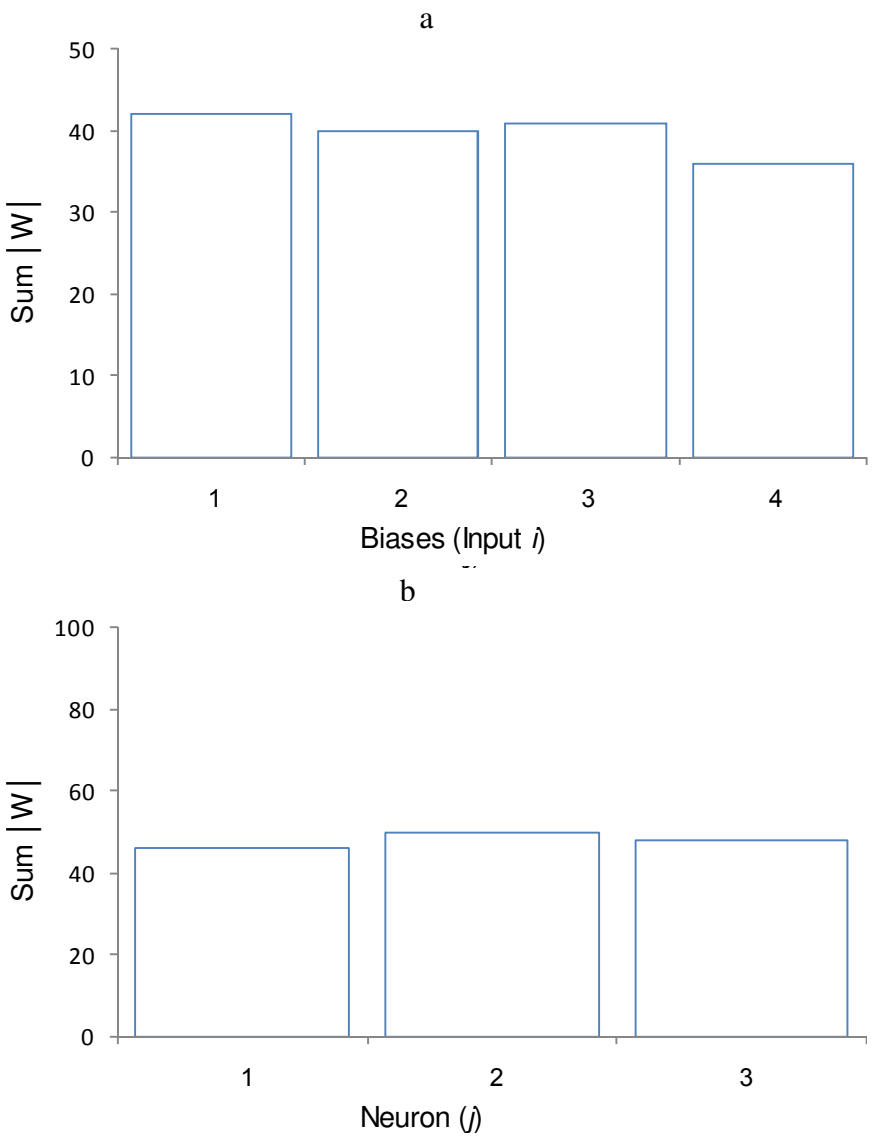

Figure 12. Final weights. (a) Sum of absolute values of the weights of four nodes in the input layer (four input nodes). (b) Sum of the absolute values of the weights of three nodes in hidden layer.

A major criticism of ANNs is their black-box aspect, since the model is constructed solely based on information obtained from the data themselves. Some attempts have been made to interpret ANN models by graphical and numerical interpretation of the hidden and input units' output (Despagne and Massart, 1988). The suggested back-propagation (Riedmiller and Braun, 1993; Riedmiller, 1994) achieves fast training when the error can be locally approximated by an open parabola and the changes of the weights can be performed independently. As the aim of the classification is to derive the border of every class, we suggested using D-optimal selection, which has proven to be slightly better (Wu et al., 1996) than other methods (example, Kennard-Stone), since the D-optimal selection selects representative training targets for the entire available data set. The main conclusions for developing training data sets are as follows:

(1). A set of data points chosen from a restricted region according to the D-optimality criterion might provide an estimation of minimum variance for the model.
(2).The quadratic polynomial is the most accurate method for approximating complex spectral features (treated as classification surfaces),
(3). Increasing the number of input nodes or observations does not drastically improve network performance.

The main difference between these two models is the basic identification as a white/black box. The LR is a white box model in which coefficient sizes determine their

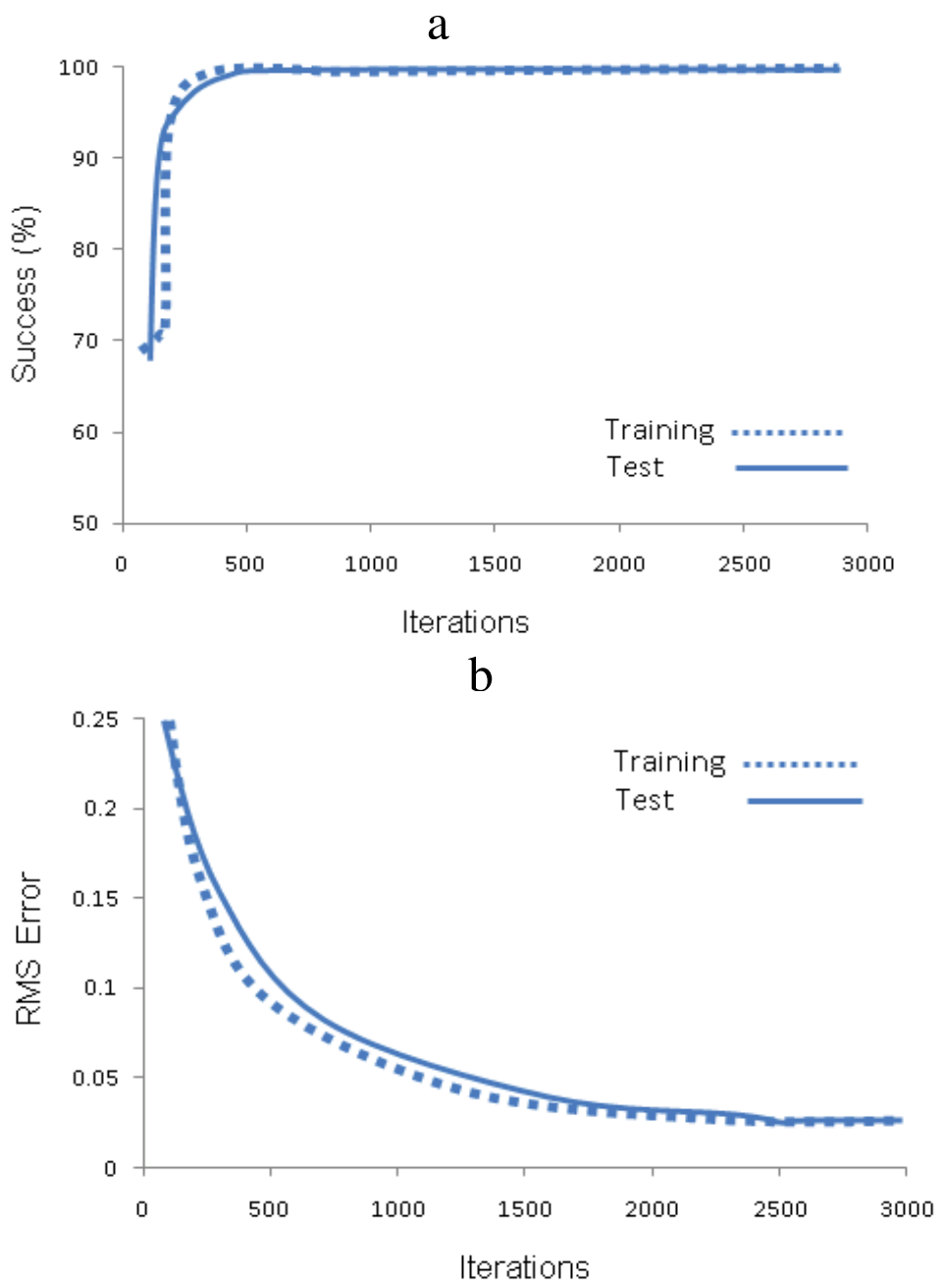

Figure 13. Network of four input, three hidden and three output nodes. (a) RMSE as a function of the number of training iterations. (b) Correctly classified targets as a function of number of training iterations.

relative importance for the classification result. In contrast, ANN is a black box model which does not allow any interaction and can only be verified externally.

Conclusion

HPC is an extremely durable and complex material including hardening, hydration and internal curing, processes which may provide additional complexity. However, measuring these processes *in situ* is complex, if not impossible. Indeed, no single method yet exists that can completely determine all chemical reactions taking place in a concrete structure from the mixing stage onward. In the present study, we suggest using the DRS technique (VIS-NIR-SWIR) for rapid assessment of the status of concrete *in situ*. This pioneering study shows that reflectance spectroscopy can be used as a promising and powerful tool to assess the concrete's status in both

Table 15. Results for back-propagation with adaptive learning and momentum.

Network	MSE	MPE	Accuracy (%)
4 × **3** × **3**	0.003	0.0009	93.21

point and spatial domains. Since the reflectance measurement is easy, rapid, and accurately obtained, it can be used in the field and provides an *in-situ* tool for engineers to inspect the concrete's status. To the best of our knowledge, this is the first attempt to show that spectral reflectance information can shed light on the concrete's quality, and if further developed, this approach could provide a unique tool for many applications in the fields of construction and building engineering.

REFERENCES

Awiti AO, Walsh MG, Shepherd KD, Kinyamario J (2007). Soil condition classification using infrared spectroscopy: a proposition for assessment of soil condition along a tropical forest-cropland chronosequence. Geoderma, 10: 2-12.

Ben-Dor E, Banin A (1995). Near infrared analysis as a rapid method to simultaneously evaluate several soil properties. Soil Sci. J., 59: 364–372.

Borggaard C, Thodberg HH (1992). Optimal minimal neural interpretation of spectra. Anal. Chem., 64: 545-551

Breiman L (2001). Random forests. Machine Learn., 45: 5-32.

Choueiki MH, Mount-Campbell CA (1999) Training data development with the D-Optimality criterion. IEEE Trans. Neural Netw., 10(1): 56-63.

Clark RN (1999). Spectroscopy of rocks and minerals, and principles of spectroscopy. Rencz N (Ed.), Remote Sensing for the Earth Sciences: Manual of Remote Sensing. John Wiley & Sons, New York, pp. 3-52.

Clark RN, Roush TL (1984). Reflectance spectroscopy: quantitative analysis techniques for remote sensing applications. J. Geophys. Res., 89: 6329-6340.

Cohn DA (1996). Neural-network exploration using optimal experimental design, Neural Networks, 9 (6): 1071-1083.

Dasarathy B (1991). Nearest Neighbor Pattern Classification Techniques IEEE Computer Society Press, Silver Spring, MD.

Despagne F, Massart DL (1988). Neural networks in multivariate calibration. Analyst, 123: 157R-178R.

Dreiseitl S, Ohno-Mechado L (2002). Logistic regression and artificial neural network classification models: a methodology review. J. Biomed. Inform., 35: 352-359.

Friedman SP, Robinson DA (2002). Particle shape characterization using angle of repose measurements for predicting the effective permittivity and electrical conductivity of saturated granular media. Water Resour. Res., 38(11): 1236-1245.

Geladi P, Dabakk E (1995). An overview of chemometrics applications in NIR spectroscopy. J. Near Infrared Spectrosc., 3: 119-132.

Grace LI, Cohen R, Dunn TM, Lubman DM, de Vries MS (2002). The R2PI spectroscopy of tyrosine: a vibronic analysis. J. Mol. Spectrosc., 215(2): 204-219.

Haar A (1910). Zur Theorie der orthogonalen Funktionensysteme. Mathematische Annalen, 69: 331-371.

Hana M, McClure WF, Whitaker TB, White M, Bahler DR (1995). Applying artificial neural networks: I. Estimating nicotine in tobacco from near infrared data. J. Near Infrared Spectrosc., 3: 133-142.

Huberty CJ, Morris JD (1989). Multivariate analysis versus multiple univariate analyses. Psych. Bull., 105(2): 302-308.

Hunt GR (1982). Spectroscopic properties of rocks and minerals. Carmichael RS (Ed.), Handbook of Physical Properties of Rocks. CRC Press, Boca Raton, FL, pp. 295-385.

Islam K, Singh B, McBratney A (2003). Simultaneous estimation of several soil properties by ultra-violet, visible, and near infrared reflectance spectroscopy. Aust. J. Soil Res., 41(6): 1101-1114.

Kokaly RF, Clark RN (1999). Spectroscopic determination of leaf biochemistry using band-depth analysis of absorption features and step-wise multiple linear regression. Remote Sens. Environ., 67: 267-287.

Ljungkrantz C, Mxller G, Petersons N (1994). Concrete Handbook Material, second ed. AB Svensk Byggtjпnst.

Lura P, Couch J, Jensen OM, Weiss J (2009). Early-age acoustic emission measurements in hydrating cement paste: evidence for cavitation during solidification due to self-desiccation. Cement Concrete Res., 39 (10): 861-867.

Malhotra VM, Carino NJ (2004). Handbook on Nondestructive Testing of Concrete, second ed. CRC Press, Boca Raton, FL.

Mualem Y, Friedman SP (1991). Theoretical prediction of electrical conductivity in saturated and unsaturated soil. Water Resour. Res., 27(10): 2771-2777.

Mutanga O, Skidmore AK (2004). Integrating imaging spectroscopy and neural networks to map grass quality in the Kruger National Park, South Africa. Remote Sens. Environ., 90: 104-115.

Mutanga O, Skidmore AK, Van Wieren S (2003). Discriminating tropical grass canopies (*Cenchrus ciliaris*) grown under different nitrogen treatments using spectroradiometry. ISPRS J. Photogramm. Remote Sens., 57: 263-272.

Osborne SD, Jordan RB, Kunnemeyer R (1997). Method of wavelength selection for partial least squares. Analyst, 122: 15631-15637.

Pudil P, Novovicova J, Kittler J (1994). Floating search methods in feature selection. Pattern Recog. Lett., 15: 1119-1125.

Quinlan R (1993). C4.5: Programs for Machine Learning. Morgan Kaufmann, Los Altos, CA.

Reeves JB, McCarty GW, Meisinger JJ (2000). Near infrared reflectance spectroscopy for the determination of biological activity in agricultural soils. J. Near Infrared Spectrosc., 8 (3): 161-170.

Reeves JB, Van Kessel JS (2000). Near-infrared spectroscopic determination of carbon, total nitrogen, and ammonium-N in dairy manures. J. Dairy Sci., 83 (8): 1829-1836.

Richardson IG (2000). The nature of the hydration products in hardened cement pastes. Cement and Concrete Compos., 22: 97-113.

Riedmiller R (1994). Advanced supervised learning in multilayer perceptrons—from backpropagation to adaptive learning algorithms. Comput. Standards Interfaces 16: 265-278.

Riedmiller R, Braun MH (1993). A direct adaptive method for faster backprogagation learning: the RPROP algorithm. In: Ruspini H (Ed.), Proceedings of the IEEE International Conference on Neural Networks. ICNN, San Francisco, CA, p. 586-591.

Ripley B (1996). Pattern Recognition and Neural Networks. Cambridge University Press, Cambridge.

Sacks J, Welch WJ, Mitchell TJ, Wynn HP (1989). Design and analysis of computer experiments. Stat. Sci., 4(4): 409-435.

Sanchez MS, Sarabia LA (1995). Efficiency of multi-layered feed-forward neural networks on classification in relation to linear discriminant analysis, quadratic discriminant analysis and regularized discriminant analysis. Chemom. Intell. Lab. Syst., 28: 287-303.

Savitzky A, Golay MJE (1964). Smoothing and differentiation of data by simplified least squares procedures. Anal. Chem., 36(8): 1627-1639.

Scholkopf B, Smola A (2002). Learning with Kernels: Support Vector Machines, Regularization, Optimization, and Beyond. MIT Press, Cambridge, MA.

Stepkowska ET (2002). Study of hydration of two cements of different strengths. J. Therm. Anal. Calorim., 69: 187-204.

Tittonell P, Shepherd KD, Vanlauwe B, Giller KE (2008). Unravelling the effects of soil and crop management on maize productivity in smallholder agricultural systems of western Kenya—an application of

classification and regression tree analysis. Agric. Ecosyst. Environ., 123: 137-150.

Udelho ̣en T, Schuttr B (2000). Capability of feed-forward neural networks for a chemical evaluation of sediments with diffuse reflectance spectroscopy. Chemom. Intell. Lab. Syst., 51: 9-22.

Welch WJ, Buck RJ, Sacks J, Wynn HP, Mitchell TJ, Morris MD (1992). Screening, predicting, and computer experiments. Technometrics., 34(1): 15-25.

Welch WJ, Yu TK, Kang SM, Sacks J (1990). Computer experiments for quality control by parameter design. J. Qual. Technol., 22(1): 15-22.

Whitney AW (1971). A direct method of nonparametric measurement selection. IEEE Trans. Comput., 20: 1100-1103.

Wise BR, Holt NB, Gallagher S, Lee A (1995). A comparison of neural networks, non-linear biased regression and a genetic algorithm for dynamic model identification. Chemom. Intell. Lab Syst., 30: 81-89.

Wold S, Sjostrom M, Eriksson L (2001). PLS-regression: a basic tool of chemometrics. Chemom. Intell. Lab. Syst., 58: 109-130.

Wong HS, Buenfeld NR (2009). Determining the water-cement ratio, cement content, water content and degree of hydration of hardened cement paste: method development and validation on paste samples. Cement Concrete Res., 39: 957-965.

Wu W, Walcmk B, Massart DL, Heuerding S, Erni F, Last IR, Prebble KA (1996). Artificial neural networks in classification of NIR spectral data: design of the training set. Chemom. Intell. Lab. Syst., 33: 35-46.

Ylmın R, Jnglid U, Steenari B, Panas I (2009). Early hydration and setting of Portland cement monitored by IR, SEM and Vicat techniques, Cement Concrete Res., 39: 433–439.

Zupan J, Gasteiger J (1991). Neural networks: a new method for solving chemical problems or just a passing phase? Anal. Chim. Acta., 248: 1-30.